SIAM J. Applied Dynamical Systems
Vol. 5, No. 4, pp. 529–551

Phase Boundaries as Electrically Induced Phosphenes*

Jonathan D. Drover† and G. Bard Ermentrout‡

Abstract. A model is presented of experiments where electrical stimulation of the eye of human subjects results in the perception of evenly spaced lines, or phosphenes. The model is a two-dimensional grid of integrate-and-fire oscillators that captures the important experimental characteristics of line-creation when a sinusoidal current injection is used. The spatio-temporal behavior of the lines, once formed, is also reproduced. A reduced model consisting of an evolution/convolution equation on the real line is analyzed, and it is shown that stationary solutions with arbitrarily located discontinuities exist and are linearly stable. Traveling waves are numerically shown to exist when the coupling is both sufficiently strong and biased, which accounts for the movement of the lines in the experiments.

Key words. phase boundaries, phosphenes, traveling waves

AMS subject classifications. 37N25, 34C15, 92B05

DOI. 10.1137/050646469

1. Introduction.

A phosphene is the sensation of light produced from within the nervous system rather than from an external source. Examples of phosphenes range from the stars seen when one is hit on the head to the geometric patterns perceived during hallucinations. Phosphenes can be induced by direct electrical stimulation of the visual pathway, including the eyeball, leading to the preliminary design of prosthetic visual devices for patients with severely limited vision [14].

Claussen [6] was the first to discover that sinusoidal electrical stimulation of the retina produced a variety of complex visual sensations. In experiments two decades later, Carpenter [4] studied these electrical phosphenes in much greater detail. If the eyeball is stimulated by high frequency (100 Hz) alternating current and a dark bar is passed through visual space, it leaves in its wake a series of thin contours which slowly move over time. These disappear almost instantly when the electrical stimulation is turned off. The production and movement of these contours is the subject of this paper.

While electrical stimulation of the eye is rather unnatural, it has recently been used to study the effects of electromagnetic radiation on the human nervous system [1]. Furthermore, Wilms et al. [23] have used direct electrical stimulation to estimate the spatial resolution of the retina as mapped onto the visual cortex. Unusual and abnormal stimuli have long been used as probes of the visual system, as they can often provide information about processing that is not available with more natural stimuli. For example binocular rivalry experiments (different images presented to the left and right eyes, leading to an alternation in the perceived

*Received by the editors November 30, 2005; accepted for publication (in revised form) by T. Kaper May 22, 2006; published electronically October 4, 2006.
http://www.siam.org/journals/siads/5-4/64646.html
†Department of Mathematical Sciences, New Jersey Institute of Technology, Newark, NJ 07102 (drover@njit.edu).
The work of this author was supported by an NSF grant while attending the University of Pittsburgh.
‡Department of Mathematics, University of Pittsburgh, Pittsburgh, PA 15260 (bard@pitt.edu).

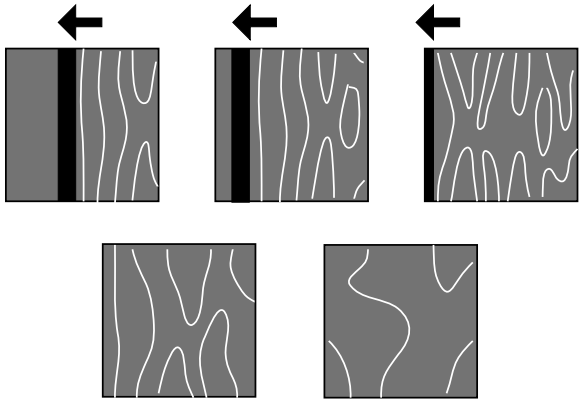

Figure 1. *The patterns reported by subjects in Carpenter's experiments (redrawn after* [4]*).*

image) led to insights into how visual forms are processed in the cortex [24]. Classic illusions such as Mach bands (illusory light or dark areas at the ends of a luminence ramp) [20] led to the theory of lateral inhibition in the retina.

In this paper, we present a new model for the formation of the so-called contour phosphenes elicited through electrical stimulation of the eyeball. Our model is based on experiments demonstrating 1:2 phase-locking of retinal cells to periodic stimuli [7], together with anatomical and physiological evidence for electrical coupling between the cells in the retina. In section 2, we introduce the experimental protocol, describe the phenomena, and introduce our model. We start with a one-dimensional (1D) system to illustrate the basic mechanism, and then turn to a two-dimensional (2D) model which reproduces both the formation of the contours and their subsequent movements. To gain better mathematical insight into the existence of contours and their stability, in section 3, we introduce a simplified 1D continuum model for which we can prove the existence of alternating domains much like those in the experiments and simulations. We prove that these are stable and also explore the onset of movement of the boundaries.

2. Electrically induced phosphenes. In this section, we model the spatio-temporal patterns reported by subjects in an experiment described in [4]. We begin by presenting a brief description of the experiment and the illusion.

A subject's eyes are submerged in a saline bath, and alternating electrical current is passed through the bath. The subject views a uniformly lit screen while receiving the stimulation. A dark object is passed through the field of vision. Subjects report line phosphenes or contours (illusions of light) in the wake of the trailing edge of the dark object. Carpenter shows that there is one line created for every complete cycle of the driving stimulus coincident with the moving edge, yielding the temporal and spatial periodicity. Thus a slowly advancing edge will produce many more lines than a rapidly advancing one. The result, upon full passage of the edge across the medium, is a set of evenly spaced line phosphenes. These lines slowly evolve in time, moving in various directions and occasionally interacting with each other to form loops (Figure 1). Later in this section, we will specify the rules of movement described in Carpenter's paper.

2.1. A model for contour formation. According to Carpenter [4] and Brindley [3], the genesis of these phosphenes is in the retina itself. This contrasts with the presumed cortical origin of more complex phosphenes seen during flicker, occular pressure, or drug ingestion [21]. Thus, we will assume that all of the dynamics are occurring within the retina.

Carpenter suggests a hypothesis as to the nature of the illusions: *The lines represent nodes, separating areas of the retina that are responding in antiphase to each other.* We take this as our main hypothesis and create a biophysically plausible implementation using recent physiological data on the retina. The basic idea is to induce bistability at each spatial location in the retina so that the phosphenes become the boundaries between the two different stable states. Given that the stimulus is periodic, one way to achieve a de facto bistability is to assume that the relevant retinal cells are able to fire only on every other cycle of the stimulus. That is, each cell is locked in a 1:2 (one spike per two stimulus cycles) manner to the 100 Hz current. Thus, the bistability is between cells firing on the "odd" cycle of the 100 Hz current and cells firing on the "even" cycle. There are many candidate cells in the retina: bipolar cells, amacrine cells, horizontal cells, and ganglion cells (whose output goes to the central nervous system). Our model does not depend on which type of cell is firing, only on the fact that the cells generating the activity are coupled. As there are electrical (gap) junctions between most of the cell types in the retina [17, 16, 15], we will not speculate as to which neurons are involved in the phosphenes as perceived in human subjects.

In [7], Crevier and Meister studied human electroretinograms (ERGs) and salamander retinal cell responses to periodic pulses of light. In the human studies, the authors found that there is a period doubling (1:2 locking) of the ERG at between 30 to 70 Hz photic stimuli. In order to explore the origin of this, these authors looked at the neurophysiology of salamander retinas since their eyes have similar structure to those of humans. They found that the photoreceptors (the first stage of vision) are able to maintain the 1:1 locking with the stimulus, but that ganglion cells (last stage in the retina) can follow only in a 1:2 manner. Thus, the inability to follow the stimulus in a 1:1 manner occurs between the photoreceptors and the ganglion cells—this includes all the cell types mentioned above: bipolar, amacrine, and horizontal.

For simplicity, we model each cell (or cluster of cells that behave identically) as an integrate-and-fire neuron with adaptation [8]:

$$\frac{dx}{dt} = -x - z + A\sin\left(\frac{2\pi t}{T}\right), \tag{1}$$

$$\frac{dz}{dt} = -\frac{z}{\tau}. \tag{2}$$

The variables x and z are real. The parameter A is the amplitude of the driving stimulus, and T is the period. We assume that both A and T are positive. The driving stimulus is the analogue to the alternating current in the experiments. The reset criterion is given by

$$x(t^-) = x_{spike} \to x(t^+) = x_{reset}; \qquad z(t^+) = z(t^-) + z_{jump}.$$

For the remainder of this section, we assume the parameter values to be $x_{spike} = \pi$, $x_{reset} = -\pi$, and $z_{jump} = 1$.

The purpose of the refractory variable, z, is to make the 1:2 phase-locking more robust. In the absence of the explicit refractory variable, the oscillations approach threshold during every cycle of the driving current, and 1:2 locking occurs only in a very narrow range of parameters. In [9] parameter regimes for 1:2 locking are explicitly found; that is, the neuron spikes exactly once for every two cycles of the current for a range of values of A. For the remainder of this paper, we assume that $A = 4.7$. Because one phase-locked solution exists, another must also exist; it is a translate of the first by one period of the stimulus. The result is a form of bistability, where the attractors are a pair of periodic orbits. A cell, after some transient behavior, will converge to one of these solutions, either the even cycle or the odd cycle. By symmetry, the basins of attraction of the two solutions have equal measure.

We now turn to the mechanism that causes the medium to break into the desired regions. We assume that, at the onset of the stimulus, the entire retinal area is simultaneously excited. Thus *all cells start in the same phase of the* 1:2 *locked solution.* All that the subject observes is a uniform background, since 100 Hz is well above the critical flicker fusion frequency of about 30 Hz. The input of a dark bar across the visual field causes the retinal receptors to depolarize. (The primary receptors in the retina act counterintuitively, since light hyperpolarizes or inhibits them.) This signal is inverted by the bipolar cells to produce spatially restricted inhibitory signal to the cells which are locked in the 1:2 rhythm with the electrical signal. This inhibition is sufficient to keep the cells from firing. Once the bar passes through, the cells are released from the inhibition and can start to fire again. Depending on the time at which they are released, they will be drawn into either the "odd" or the "even" 1:2 locked solution. All cells aligned in parallel with the bar of light will be released simultaneously, so that all cells in the vertical direction will have the same phase. Thus, to understand the initial creation of the phase-boundaries, we need consider only a 1D line of cells through which sweeps an inhibitory pulse.

We model this inhibition using a step function

$$\text{bar}(i,t) = \begin{cases} -d & \text{if } i/v + T_0 < t < i/v + T_0 + W, \\ 0 & \text{otherwise,} \end{cases} \tag{3}$$

where i is the index of the node, T_0 is the time when the sweep begins, W is the amount of time that a node is inhibited, and v is the velocity of the sweep. The parameter d is the strength of the inhibition.

We first consider a horizontal line of cells with the inhibitory sweep. The variable x_i at location i satisfies

$$\frac{dx_i}{dt} = -x_i - z_i + A\sin(\omega t) + \text{bar}(i,t) \equiv F_i(x_i, z_i, t). \tag{4}$$

The creation of the lines occurs in the wake of the traveling inhibition. Prior to the sweep, the visual field is uniform, and all cells are phase-locked to the driving stimulus. The traveling inhibition causes the nodes to deviate from the phase-locked solution. The inhibition is sufficiently long so that, upon the completion of a sweep, approximately half of the nodes are left in the basin of attraction corresponding to the opposite phase solution. Because the inhibition travels with a constant velocity, once the inhibition has passed, the medium has alternating regions firing in the odd and even cycles. The locations where there is a phase

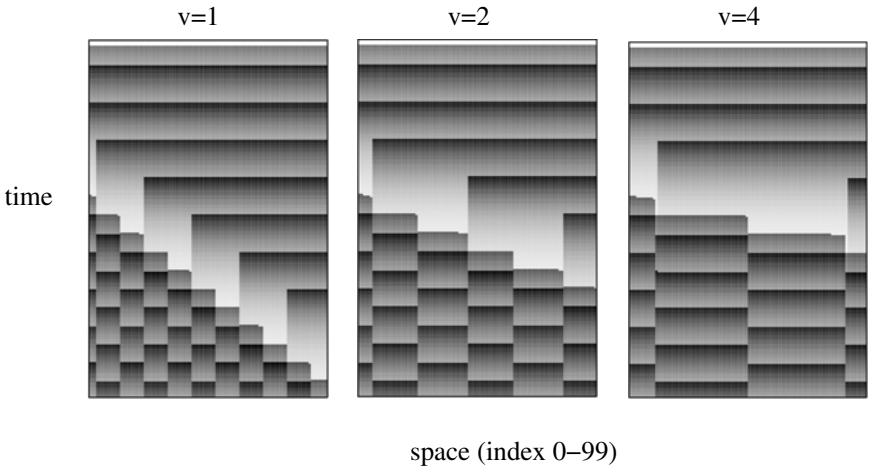

Figure 2. *Three simulations of a line of oscillators inhibited by a sweep of the bar function. In each panel the horizontal axis is the spatial index, and the vertical axis is time, increasing from top to bottom. Grayscale represents the value of the refractory variable, z_i. The velocity of the sweep is above each panel and measures the speed of the movement of the bar in index units per time. In all three panels $W = 30$ and $d = -2$.*

boundary correspond to the phosphenes in Carpenter's experiment. The phase-locked solutions have identical basins of attraction, and so the result is the appearance of evenly spaced phase boundaries. In Figure 2, the behavior of the line of oscillators is shown during and after a sweep. In Carpenter's experiments, one line was seen for every cycle of the stimulus coinciding with the trailing edge of the bar. Thus, the slower the bar moves, the more lines. In this figure, $T = 10$. For $v = 1$, there are ten cycles of the stimulus, and there should be 10 lines. Similarly, for $v = 2$ and $v = 4$, there should be 5 and 2–3 lines, respectively. These simulations confirm that our model behaves appropriately. Furthermore, the thickness of the contours is independent of the velocity of the bar. This suggests that the contours are *not* different states of the system, but rather, they are the *boundaries* between two stable states. We next model the movement of these boundaries.

2.2. Movement of the lines: Two dimensions. The previous section provided a simple but robust mechanism for partitioning a 1D "retina" into regularly spaced domains of alternating phase. Suppose, for the moment, that our situation is exactly as in section 2.1, where all the cells are uncoupled and independent, but now arranged in a 2D grid. A stimulus in the form of a long vertical bar is moved horizontally across the 2D array of cells. All cells in any column will behave exactly the same since the bar is vertical. After the bar passes, it will leave a series of vertical stripes representing the alternating domains of in- and out-of-phase oscillations much like those shown at the leading edge of the stimulus in Figure 1. However, in the experiments, the lines do not remain fixed. Rather, they move and appear to interact with each other. In this section, we suggest that the reason for the movement is that there are interactions between the neighboring cells which underlie the phosphene patterns.

Carpenter makes the following observations about the phosphenes:

1. Lines never cross through one another. Rather, they combine to form loops.
2. A line never breaks apart unless it meets another line.

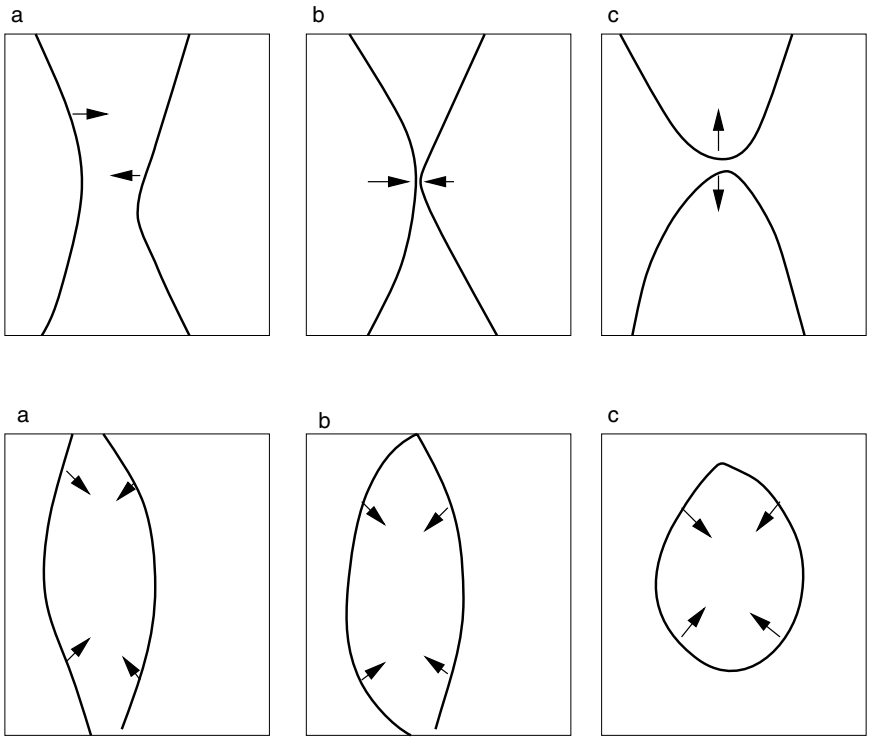

Figure 3. *Line behavior when two lines meet. The top panel depicts the case where the lines meet near their centers. The bottom panel is the case where the lines meet near the edges. In either case, the lines do not pass through one another, but instead leave patterns similar to those shown.*

3. Neighboring lines show a tendency to move in a similar manner. That is, if a given line is bulging to the right, then it is likely that a neighboring line will bulge in the same direction.

Figure 3 illustrates the first two rules.

In the model as posed so far, each cell is independent from the others, and there are no interactions. Furthermore, the model is completely homogeneous. However, there are many interactions between retinal neurons—graded chemical synapses, electrical junctions, threshold chemical synapses, etc. Thus, we can expect that, at least locally, the behavior of one neuron will influence that of another one. The detailed means of coupling is less important than its effect. We will assume that coupling is such that two coupled neurons will tend to synchronize their activities. As there is much evidence for electrical (gap) junctions in the retina [17, 15] and since such coupling can synchronize neuronal oscillations [13, 19], we will illustrate the phenomena with gap junction coupling. We note that gap junction coupling is generally modeled as a linear function of the difference between the potentials of two cells: discrete diffusion.

Coupling provides a mechanism for the first two of Carpenter's observations. (See Figure 4.) Within a domain, all cells are nearly equal and firing at the same cycle, so that in the interior the coupling has a negligible effect. However, a point near the boundary will try to synchronize with cells which are firing on opposite phases of the stimulus. With perfectly

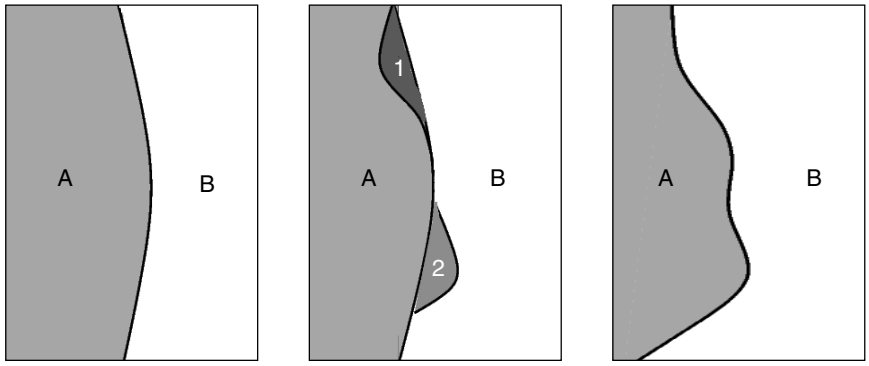

Figure 4. *Line movement mechanism. The figure depicts three moments in time, advancing from left to right. In the leftmost, the boundary is shown separating regions that are out of phase with one another. In the center of the figure, the region marked* 1 *is more strongly coupled to the cells in region B than to those in region A. The opposite is true for those cells in region* 2*. The right of the figure shows the result once the cells in region* 1 *have synchronized with those in region B and the cells in region* 2 *have synchronized with region A. This is how line movement occurs in our model.*

symmetric coupling, the battle is a "tie." However, if the coupling has any kind of asymmetry (which is generally the case), then the boundary point will be recruited into the region with the stronger effective coupling, thus moving the boundary point; one region will take over the other, and the lines will move away from the absorbing area. In the uncoupled case, the pattern is stable so that the coupling has to be sufficiently strong to begin the process of recruiting territory. In order to explain rule 3, we have to make a somewhat stronger assumption about the coupling heterogeneity. If the heterogeneity is at a "microscopic" scale, that is, essentially random from cell to cell, then we cannot expect any kind of trend in motion such as seen in Figure 4. Thus, we suppose that the coupling strength varies on a coarser scale. If the coupling has a favored direction at some point x, then nearly the same direction will be favored for a point y near x. We have no evidence of such trends in coupling, but, neither is there any compelling evidence against this. This notion could be tested by looking for any kind of asymmetry of spontaneous wave propagation in isolated retinas [12].

2.2.1. Line movement and biased coupling strength. We assume that coupling within the retina, particularly the gap junctions between horizontal cells, is not of uniform strength. We accomplish the movement of the lines by coupling a given node to its neighbors with different strengths. Since the effect of the coupling is to synchronize, a cell will approach the phase of the neighbor to which it is most strongly coupled (see Figure 6 below). It is through this mechanism that cells on a boundary synchronize with neighbors, moving the boundary itself (Figure 4).

The coupling has to have a number of characteristics, inspired by the movement "rules" stated in the previous subsection. Rules 2 and 3 make it essential that the coupling cause synchrony to be a locally stable solution. The most obvious form of coupling would be to add a term proportional to the difference between the x components of the two cells, e.g., $x_2 - x_1$. This form of coupling works very well for a pair of coupled cells and, if sufficiently strong, induces synchrony [19]. However, we have found (simulations not shown) that linear coupling

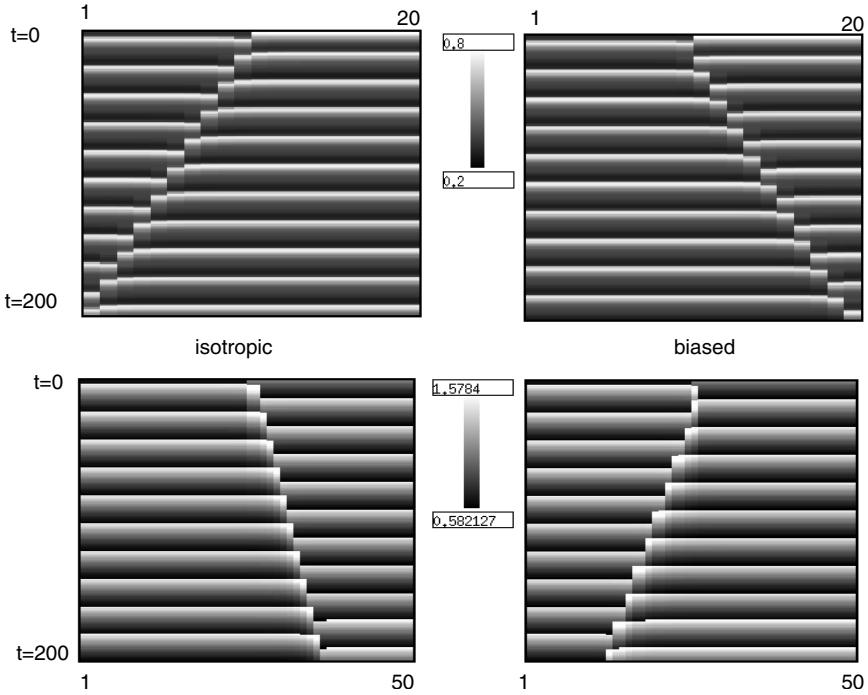

Figure 5. *Behavior of a forced array of Hodgkin–Huxley neurons (top row) with isotropic and biased linear diffusional coupling. Bottom row: Integrate-and-fire model with sinusoidal coupling, with and without bias.*

of the integrate-and-fire model in spatially organized arrays of cells does not lead to smooth patterns in which one phase takes over the other. Rather, the medium breaks up into very fine-grained spatial patterns. Thus, we do not use linear coupling between the cells, but instead coupling which depends on the sine of the difference. To justify this somewhat unusual form of coupling, we compare a 1D integrate-and-fire network with sinusoidal coupling to a 1D network of periodically forced Hodgkin–Huxley neurons. Each cell satisfies the four variable Hodgkin–Huxley equations and is forced at 100 Hz by a sinusoidal stimulus with amplitude sufficient to lead to 1:2 locking. Cells are coupled to nearest neighbors with identical coupling to the left and right cells or with a bias in one direction. Figure 5 shows a simulation when the coupling is strong enough to destroy the two-phase pattern. When the medium is isotropic, a wave is generated, and it is always in the same direction (top left). By biasing the coupling strength, we can make the wave travel in the opposite direction (top right). The same phenomenon is illustrated with the integrate-and-fire model with sinusoidal (as opposed to linear) coupling. Since this is the type of behavior we are looking for, we use sinusoidal coupling instead of linear coupling for the integrate-and-fire model.

With these considerations, we return to the full 2D model and use coupling of the form

$$cf_d \sin(x_d - x_{i,j}), \tag{5}$$

where $d = \{up, down, left, right\}$ (e.g., $f_{up} = f_{i,j-1}$). See Figure 6. The coefficients f_d are positive and discussed in detail in the next subsection. We restrict ourselves to the case of nearest neighbor coupling, although in the next section longer range coupling is allowed. The

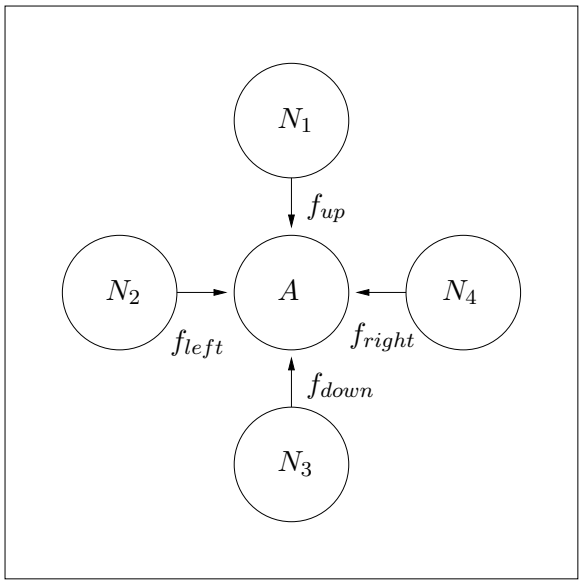

Figure 6. *Coupling diagram.*

parameter c is always positive and determines the linear strength of the coupling, and it is the same for each node. The evolution of the cells in the coupled network is governed by the equation

$$\frac{dx_{i,j}}{dt} = F_{i,j}(x_{i,j}, z_{i,j}, t) + c\sum_d f_d \sin(x_d - x_{i,j}), \tag{6}$$

where $F_{i,j}(x, z, t)$ is the local dynamics from (4) along with the dynamics for the refractory variable governed by (2) and the sum is over the four nearest neighbors. The 1D bar in (4) is replaced by the corresponding rightward moving vertical bar in the 2D system.

2.2.2. The coupling coefficients f_d. To motivate our choice of coupling, we briefly discuss the mechanism for movement of the phosphenes. Suppose that we have one oscillating cell, A, with four neighbors, N_j, $j = 1, \ldots, 4$ (Figure 6). Suppose that N_1 and N_2 are firing synchronously (with one another), and N_3 and N_4 are firing at the opposite phase. The phase to which A synchronizes depends on the relative strengths of the coupling. For example, suppose that $f_{up} + f_{left} \gg f_{right} + f_{down}$. Then, oscillating cell A will synchronize with N_1 and N_2. If the relative difference between coupling strengths is not so high, there will be an intermediate phase for A, which will in turn alter other nearby cells. Eventually, cell A will be on the interior of a region and will synchronize with the others there. The phosphenes are represented by the boundaries of regions which have different phases where they temporarily assume a parameter dependent (relative sizes of f_d), and neighbor dependent, phase and are then absorbed into the interior of a region. Once this process is complete, the line (boundary) will have moved.

Because the direction of the movement depends on the relative coupling strengths, we wish to structure the coefficients, f_d, spatially. Suppose we have a single line of oscillators. If

for every oscillator $f_{right} > f_{left}$, we expect each to synchronize with its neighbor to the right, thus moving the lines left.

From rule 3, neighboring lines tend to move in the same direction, so there should be spatial intervals in which coupling in a particular direction is favored. Thus, rather than choosing the coupling strengths independently at each spatial point, we allow them to vary in a continuous fashion. For example, if $f_{up} > f_{down}$ at location x, then the same inequality will hold for nearby oscillators. The particular choice of coupling parameters is not crucial; however, continuity is needed to satisfy rule 3. The specific coupling matrix is described in the next section.

Bias in the coupling strength plays an important role in the movement of the phosphenes. Figure 5 shows that, without bias, the phosphenes move in one direction. In particular, for the Hodgkin–Huxley model, one cycle (say the even) always takes over the other if the coupling is sufficiently strong. The reason for this (similarly for the integrate-and-fire model) is as follows. Consider a pair of uncoupled cells which are firing on alternate cycles. Turn on the coupling at a time t. If the coupling is strong enough, the cell that fires first after t will cause the other cell to fire, and thus the second cell will be pushed into firing in the same cycle as the first cell. In a network in which half the cells are set in the even and the other half in the odd cycle, the moment the coupling is turned on will determine the direction of the wave. This is an exquisite sensitivity to initial conditions as well as any small heterogeneities. Thus, by making the medium anisotropic, we allow waves that robustly travel in a preferred direction.

2.3. Simulation. Simulations were done using a fourth order Runge–Kutta integrator with constant time step, $\Delta t = 0.01$. The reset is accomplished by setting $x_{i,j}(t_k) = -\pi$ and $z_{i,j}(t_k) = z_{i,j}(t_k) + 1$ whenever $x_{i,j}(t_k) > \pi$. No interpolation is done, resulting in resets that always occur at a multiple of the time step.

All simulations are done on a 100×50 grid. The coupling strength array, $f_{i,j}$, was determined as follows:

1. Randomly choose three indices in the horizontal domain (h_1, h_2, h_3), and three more in the vertical domain (v_1, v_2, v_3). Assume that $h_1 < h_2 < h_3$ and $v_1 < v_2 < v_3$. The choice of three set indices is motivated by figures in [4]. This implementation can be extended to incorporate any number of set nodes, up to the number of nodes present in the grid.
2. Define two arrays, H and V (for horizontal and vertical), with the appropriate number of elements. For our purposes H has 100 elements (the width of the grid) and V has 50 elements (the height of the grid).
3. Assign to the array elements $H(1)$, $H(h_1)$, $H(h_2)$, $H(h_3)$, and $H(100)$ random values between 0 and 1.
4. The grid is now divided into rectangles. Divide each of these rectangles into two right triangles. In the simulations presented here, the diagonal goes from the top left to the lower right.
5. Using the three corners of the triangles, compute the value at the indices inside each triangle according to the plane the corner values define (see Figure 7).

We assume (as noted above) that there are heterogeneities in the retina, but at a coarse scale that covers many cells so that coupling strengths have some spatial correlations. While the

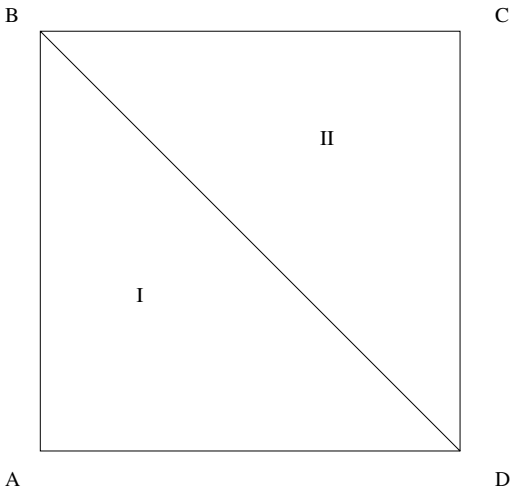

Figure 7. *A diagram that shows how the biased coupling is determined for the simulations. The value of the function is chosen randomly at the vertices A, B, C, D. The rectangle is divided into two triangles. The value of the coupling function for points in these triangles is determined using a linear interpolation of the three vertices that form the triangle. For example, if a node lies in the region marked II, the value of the relative coupling strength at that node is determined by the plane that crosses the determined points at B, C, and D.*

evidence for such large-scale heterogeneities is unclear (Marla Feller, personal communication, and [12]), by carefully looking at spontaneous propagating waves in isolated retinas, it may be possible to test this hypothesis.

Simulations were carried out using FORTRAN code, with calls to LAPACK and BLAS to do the vector operations in the Runge–Kutta integrator. The graphical output was produced using the PGPlot package. Because we use an integrate-and-fire model, we plot the recovery variable, $z_{i,j}$, as this is continuous.

Figure 8 shows output from a sample run of the simulation. In panel A, the bar (outlined in a thin dashed line) is about to complete the pass to the right. Lines (or regions) have formed on the left edge and have begun to move. In panels B and C, the lines are clearly defined and moving. In panel D, synchronous regions "poke holes" through a region in antiphase, forming two loops. Panels E and F show two of the loops annihilating themselves as the region that defines them collapses. Compare this with Figure 1.

3. A bistable evolution/convolution network. The analysis of the formation of domains, their transient stability, and the onset and direction of movement is a difficult task, given that each "cell" is governed by a nonlinear periodically driven 2D differential equation. Hence, it is useful to introduce a heuristic model which has similar qualitative features. In this section, we consider such a simplified model for the spatial network for which we can prove the existence of local phase-domains. The simple model also provides insight into the movement of the boundaries between domains and how the transition between stationary and moving patterns is effected. We will concentrate on a 1D network since this is conceptually easier to understand. However, the theorem in [2] is independent of the spatial dimension and applies, in particular, to 2D domains. The result proved below is an extension of [2], so that, with little effort, a 2D version of it is likely to hold.

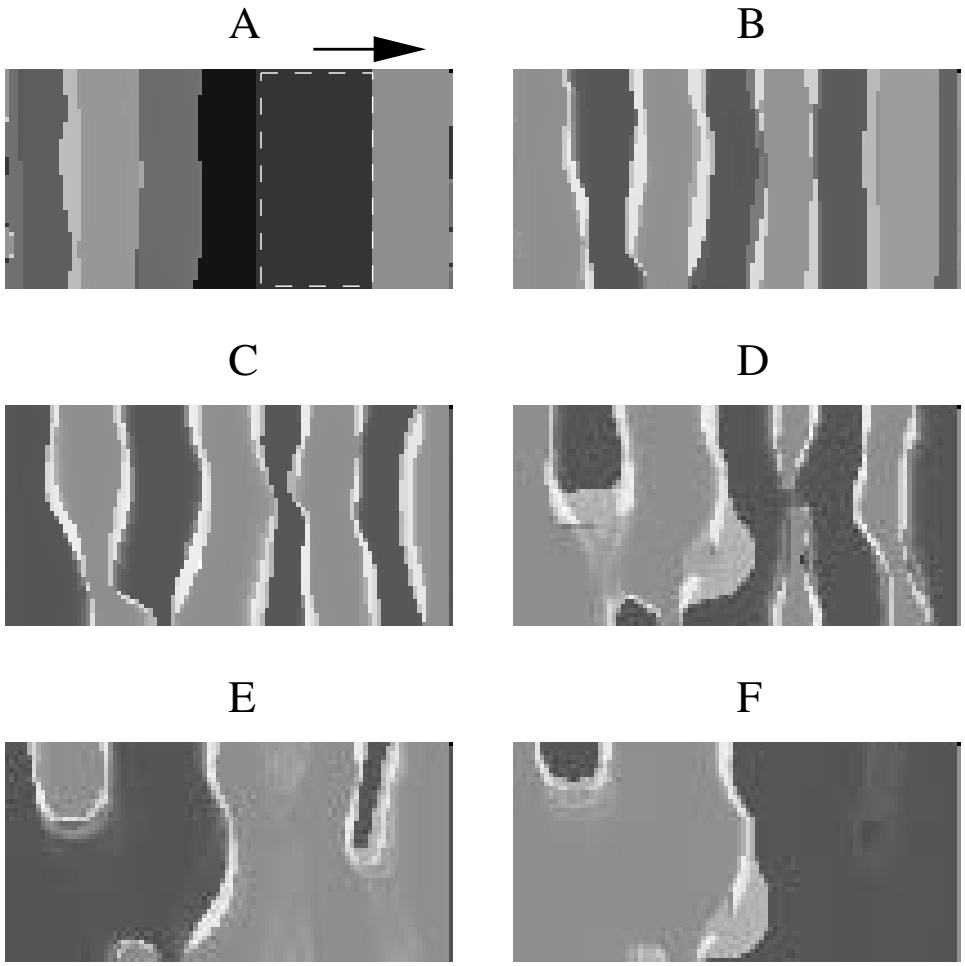

Figure 8. *Simulation of the integrate-and-fire model on a* 100×50 *oscillator grid. Each panel shows the field after a set increment of time. The variable plotted is* z*, the refractory variable. Parameter values (for* (6)*) are* $v = 1.3$*,* $A = 4.7$*,* $T = 10$*,* $\tau = 20$*,* $d = -2$*,* $W = 30$*,* $c = 7$*. Clicking on the above image displays the accompanying animation of simulated phosphenes* (64646_01.mpg [2.93MB]).

3.1. Derivation. The integrate-and-fire model with adaptation is an excitable system. With sufficiently strong periodic drive, each cell can be driven to fire at every other cycle. Conceptually, in the absence of coupling we can represent the dynamics of each cell by a scalar variable depicting its phase relative to the firing time of the stimulus. The period of the stimulus is T, but since each cell is firing only at every other cycle, the period of an individual cell is $2T$. Thus, the individual dynamics of each cell can be written in terms of the scalar variable as

$$u_t = H(u). \tag{7}$$

Zeros of $H(u)$ correspond to times with respect to the stimulus at which the cell fires. The function $H(u)$ should be T-periodic, so that if $u = \bar{u}$ is a fixed point, $H(\bar{u}) = 0$, then there

will be a second fixed point, $u = \bar{u} + T$, corresponding to u firing on the opposite cycles of the stimulus. Thus, on the interval $[0, 2T)$, there is bistability corresponding to firing on the even and odd cycles of the periodic stimulus. Furthermore, we want $\bar{u}$ to be the only stable fixed point in the interval $[0, T)$. An exact scalar equation of the form (7) can be derived from the integrate-and-fire with adaptation model if we assume that the unforced system is an intrinsic oscillator and the forcing has roughly twice the same frequency [10]. However, in the present situation, the forcing is strong and the unforced model is excitable. Thus (7) should be viewed as a simplified version of the forced excitatory cell.

Now, consider two neighboring cells which are coupled by gap junctions, that is, coupling depending only on the difference between, say, the voltages of the cells, and which vanishes when the cells are in identical states. Since $u \in [0, 2T)$, the coupling function must be $2T$-periodic. Furthermore, if both cells are in the same state, then the coupling should not contribute anything to the dynamics since the coupling is diffusion-like. This leads us to the following simplified equation for a pair of coupled cells:

$$\begin{aligned} u_1' &= H(u_1) + cD(u_2 - u_1), \\ u_2' &= H(u_2) + cD(u_1 - u_2), \end{aligned} \tag{8}$$

where H is T-periodic and D is $2T$-periodic. Before turning to the analysis of the continuum model, let us consider a simple example illustrating the general phenomena. Suppose that $T = 2$ and choose $H(u) = \sin \pi u + a \cos \pi u$ and $D(u) = \sin(\pi u/2) + q(1 - \cos(\pi u/2))$. Note that we have included cosine terms in the equations for H, D since we cannot assume any kind of intrinsic symmetry in the functions, as this can destroy the genericity of the results [18]. For small a, $u_1 \approx 1$ and $u_2 \approx -1 \equiv 3$ is a fixed point when $c = 0$. Thus u_1 fires on even cycles of the stimulus and u_2 fires on odd cycles. For c small enough this stable fixed point persists. However, for $c > c^*$, this state is lost via a saddle-node bifurcation (not shown, but see Figure 10 for a higher-dimensional analogue), and the system synchronizes at $u_1 = u_2 \approx 1$ or $u_1 = u_2 \approx -1$. That is, one domain takes over the other.

If we now imagine an array of cells arranged on a line with local coupling which can extend beyond nearest neighbors, then we obtain the following generalization of (8):

$$u_j' = H(u_j) + c \sum_k J_{j-k} D(u_k - u_j), \tag{9}$$

where J_k is a nonnegative weight for the strength of coupling. Since the strength of electrical junctions falls off with distance [13], we assume the same about J_k. Proceeding to the continuum limit, we obtain

$$\frac{\partial u}{\partial t}(x,t) = H(u(x,t)) + c \int_{\mathbb{R}} J(x-y) D(u(y,t) - u(x,t)) dy, \tag{10}$$

which we analyze in the next section.

3.2. Behavior of the continuum model. In this and the succeeding sections, we analyze (10), where $u : \mathbb{R} \times (0, \infty) \to \mathbb{R}$. The parameter c is real and positive. The function H is continuously differentiable and periodic with period T. The function D is continuously

differentiable and periodic with period $2T$. We assume, without loss of generality, that $T = 2$. Additionally, the functions satisfy

$$H(-1) = H(0) = 0,$$

$$H'(-1) < 0,$$

$$H'(0) > 0,$$

$$D(0) = 0,$$

$$D'(0) > 0.$$

The conditions on H and D guarantee that each is bounded and well defined on the entire real line. Thus, solutions to the initial value problem with $u(x, 0)$ evolving according to (10) will not blow up in finite time. Also, since the right-hand side of (10) is always defined, the first time derivative of u exists for all $t > 0$, and so the solutions will be continuous in t. In other words

$$\lim_{\Delta t \to 0} u(x, t + \Delta t) - u(x, t) = 0$$

for every $x \in \mathbb{R}$.

In [2], the authors prove the existence and stability of stationary solutions to

$$u_t = -u - \lambda f(u) + J * u, \tag{11}$$

where $\lambda > 0$, $J * u$ is the spatial convolution of J with u, and the function f is bistable. Specifically, they prove that, under conditions on the parameters, there exist stable steady state solutions that are discontinuous. In this section we prove the existence of similar solutions to (10). We remark that the proofs of existence and stability do not depend at all on the fact the the model is on a 1D domain. Indeed, all proofs hold in arbitrary domains and, in particular, the planar domain of the simulations. We focus on the 1D case, as the proof is easier to explain.

3.3. Existence of stationary solutions. We wish to prove the existence of stationary solutions that are discontinuous at arbitrary points on the real line. We begin by choosing a set, M. Denote the complement by M^c. Also, choose $\beta > 0$ such that $H'(u) < 0$ for all $u \in (1 - \beta, 1 + \beta)$. We wish to prove the existence of a solution, $U(x)$, satisfying

$$0 = H(U(x)) + c \int_{\mathbb{R}} J(x - y) D(U(y) - U(x)) dy \tag{12}$$

with

$$U(x) \in (1 - \beta, 1 + \beta) \quad \text{when } x \in M,$$

$$U(x) \in (-1 - \beta, -1 + \beta) \quad \text{when } x \in M^c.$$

We assume that the function H satisfies the following conditions:

- H is a periodic function with period 2,
- H is continuously differentiable,
- $H(1) = 0$ and $H'(1) < 0$,
- $H(0) = 0$ and $H'(0) > 0$,

and that the function D satisfies

- D is continuously differentiable,
- $D(0) = 0$ and $D'(0) > 0$,
- D is periodic with period 4 (twice the period of H).

These conditions are consistent with the analogy to the full integrate-and-fire model. Specifically, the 2-periodicity of H reflects the symmetry of the medium. In the full model, each of the pair of stimulus-induced basins of attraction were identical. Since the function H describes the intrinsic properties for a given point on the line, it is appropriate to assume higher periodicity than for D. The condition that H be continuously differentiable is for convenience in the proof that follows. The conditions on the function D reflect the properties of the coupling. The full model was developed under the assumption that the coupling encourages synchrony between neighboring cells. Since D depends on the difference in u, the $D'(0) > 0$ condition follows easily (as this is equivalent to *positive* diffusion). Also, cells that are synchronized have no effect on one another, which leads to the condition that $D(0) = 0$. Finally, the choice of fixed points of H is arbitrary and for convenience.

Let $\beta > 0$ be a number such that $H'(u) < 0$ for $u \in (1-\beta,\ 1+\beta)$, and set $\delta = -\max_{u\in(1-\beta,1+\beta)} H'(u) > 0$. Set $K = \max_{u\in\mathbb{R}} |D'(u)|$. Choose a measurable set M and denote the complement as M^c. Assume that c is small enough so that the following conditions hold:

$$
\begin{aligned}
H(1+\beta) + c\overline{D}_{MM^c} \sup_{x\in M} \int_{M^c} J(x-y)dy &\le 0,\\
H(1-\beta) + c\underline{D}_{MM^c} \sup_{x\in M} \int_{M^c} J(x-y)dy &\ge 0,\\
H(-1+\beta) + c\overline{D}_{MM^c} \sup_{x\in M^c} \int_{M} J(x-y)dy &\le 0,\\
H(-1-\beta) + c\underline{D}_{MM^c} \sup_{x\in M^c} \int_{M} J(x-y)dy &\ge 0,
\end{aligned}
\tag{13}
$$

where

$$
\overline{D}_{MM^c} = \max_{s\in(2-2\beta,2+2\beta)} D(s),
$$

$$
\underline{D}_{MM^c} = \min_{s\in(2-2\beta,2+2\beta)} D(s).
$$

These conditions quantify the competition between the intrinsic properties at a location and the coupling influence on that location. They are derived by choosing a band of width β around the stable equilibria of $u' = H(u)$ and comparing the strength of attraction with the maximum possible strength of the coupling toward the opposite equalibrium. These conditions

guarantee that the coupling strength, c, is not strong enough to force a uniform profile across the entire line for any set M, where

$$u(x,0) \in \begin{cases} (-1-\beta, -1+\beta) & \text{for} \quad x \in M, \\ (1-\beta, 1+\beta) & \text{for} \quad x \in M^c. \end{cases}$$

We can now state the following theorem.

Theorem 1 (existence). *Define δ and K as above, and assume that H and D satisfy the conditions described above. Also assume that (13) holds. If $-\delta + 2cK < 0$, then there exists a solution, $U(x)$, satisfying*

$$0 = H(U(x)) + c\int_{\mathbb{R}} J(x-y)D(U(y)-U(x))dy \tag{14}$$

such that

$$\begin{aligned} U(x) &\in (1-\beta, 1+\beta) \quad \text{when } x \in M, \\ U(x) &\in (-1-\beta, -1+\beta) \quad \text{when } x \in M^c. \end{aligned} \tag{15}$$

Proof. Let

$$B = \left\{ U(x) \;\middle|\; \begin{array}{rcl} U(x) \in (1-\beta, 1+\beta) & \text{when} & x \in M \\ U(x) \in (-1-\beta, -1+\beta) & \text{when} & x \in M^c \end{array} \right\}$$

and define the map

$$TU(x) = U(x) + \epsilon\left[H(U(x)) + c\int_{\mathbb{R}} J(x-y)D(U(y)-U(x))dy\right]. \tag{16}$$

For ϵ sufficiently small, the conditions (13) guarantee that $T : B \to B$. Our method of proof is to show that T is a contraction mapping. This allows us to conclude that there is a solution of the type (15) that satisfies (14).

To simplify expressions, define the function

$$A(U,x) = \int_{\mathbb{R}} J(x-y)D(U(y)-U(x))dy.$$

Let $U, V \in B$. We write

$$\|TU - TV\|_\infty = \|U - V + \epsilon(H(U) - H(V) + A(U,x) - A(V,x))\|_\infty.$$

The quantity $A(U,x) - A(V,x)$ can be written

$$\int_{\mathbb{R}} J(x-y)[D(U(y)-U(x)) - D(V(y)-V(x))]dy.$$

Because D is continuously differentiable and K is a finite number, we have that

$$|D(g-h)| < K|g-h|$$

for $g, h \in \mathbb{R}$. We have the inequality

$$\begin{aligned}\|A(U,x) - A(V,x)\|_\infty &\leq \left\| cK \int_{\mathbb{R}} J(x-y)(U(y) - U(x) - V(y) + V(x))dy \right\|_\infty \\ &= \left\| -cK(U(x) - V(x)) \int_{\mathbb{R}} J(x-y) + cK \int_{\mathbb{R}} J(x-y)(U(y) - V(y))dy \right\|_\infty \\ &\leq cK \int_{\mathbb{R}} J(x-y)dy \|U(x) - V(x)\|_\infty + cK \int_{\mathbb{R}} J(x-y)dy \|U(x) - V(x)\|_\infty \\ &= \left(2cK \int_{\mathbb{R}} J(x-y)dy \right) \|U(x) - V(x)\|_\infty.\end{aligned}$$

We may write

$$\|TU - TV\| \leq \|U(x) - V(x) + \epsilon(H(U(x)) - H(V(x)))\| + 2\epsilon cK\|U(x) - V(x)\|. \tag{17}$$

Since $H'(U) > -\delta$ for $u \in (1-\beta, 1+\beta)$ we have that

$$H(U(x)) - H(V(x)) \leq -\delta(U(x) - V(x)) \leq 0$$

for x such that $U(x) > V(x)$ and

$$0 \leq H(U(x)) - H(V(x)) \leq -\delta(U(x) - V(x))$$

for x such that $U(x) < V(x)$. Since the value of $H(U(x)) - H(V(x))$ has the opposite sign as $U(x) - V(x)$ it follows that

$$\|U(x) - V(x) + \epsilon(H(U(x)) - H(V(x)))\|_\infty \leq \|U(x) - V(x) - \epsilon\delta(U(x) - V(x))\|_\infty. \tag{18}$$

We may choose ϵ small enough so that $\epsilon\delta < 1$. Substituting (18) into the right-hand side of (17) gives

$$\begin{aligned}\|TU - TV\|_\infty &\leq (1 - \epsilon\delta)\|U(x) - V(x)\|_\infty + 2\epsilon cK\|U(x) - V(x)\|_\infty, \\ \|TU - TV\|_\infty &\leq (1 - \epsilon(\delta - 2cK))\|U(x) - V(x)\|_\infty.\end{aligned}$$

Thus, if $\delta > 2cK$, then T is a contraction mapping, and hence there is a steady state solution to (10).

The quantity $-\delta + 2cK$ is a comparison of the strength of the attraction to the stable fixed points of the function H to the strength of the coupling. If δ is sufficiently large, then the attraction to the stable roots of H is strong enough to counter the coupling. On the other hand, for strong enough coupling, the network will assume a more uniform profile and the solutions will not remain in bands of width β around the fixed points for the uncoupled system.

It is important to note that Theorem 1 provides sufficient conditions for the existence of these solutions; however, they are not, in general, necessary. The Lipschitz condition used to bound the effect of the coupling can be somewhat generous, given that the solutions lie in the β bands.

We remark that the existence proof is virtually identical to that in [2]; our diffusion function is somewhat different, but once we impose the Lipschitz condition, the proof proceeds identically.

3.4. Stability. We now prove stability of the above patterns with the same hypotheses as needed for their existence.

Theorem 2 (linear stability). *Assume that for a set M, a number β, and a parameter c the conditions in Theorem 1 are satisfied. The resulting stationary solution is linearly stable.*

Proof. Let $U(x)$ be the steady state solution to (10). Linearizing around the steady state, we obtain

$$\partial_t w(x,t) = H'(U(x))w(x,t) + c\int_{\mathbb{R}} J(x-y)D'(U(y)-U(x))[w(y,t)-w(x,t)]dy. \tag{19}$$

We rewrite (19) as

$$\partial_t w(x,t) = f(x)w(x,t) + c\int_{\mathbb{R}} J(x-y)D'(U(y)-U(x))w(y,t)\ dy,$$

where

$$f(x) = H'(U(x)) + c\int_{\mathbb{R}} J(x-y)D'(U(x)-U(y))\ dy.$$

We know that $H'(U(x)) < -\delta$ for all x, and D is Lipschitz with constant K. Thus, $f(x) < -\delta + cK \equiv -b$ for all x, and if c is small enough, then $-b < 0$. Taking absolute values, we see that $|w(x,t)|$ is less than $v(x,t)$, where $v(x,t)$ is nonnegative and satisfies

$$v_t = -f(x)v(x,t) + cK\int_{\mathbb{R}} J(x-y)v(y,t)\ dy.$$

Here we have used again the fact that D is Lipschitz and also that $J(x-y)$ is nonnegative. The right-hand linear operator clearly preserves nonnegativity. Consider the following equation:

$$z_t = -bz(x,t) + cK\int_{\mathbb{R}} J(x-y)z(y,t)\ dy. \tag{20}$$

Solutions to this problem can be found with Fourier transforms. Since $J(x) \geq 0$ and is symmetric and integrable, the Fourier transform, $\hat{J}$, exists, is real, and is less than or equal to $\hat{J}(0) = 1$. Solutions to (20) have the form $z(x,t) = \exp(\lambda t + i\ell x)$, where ℓ is real and

$$\lambda = -b + cK\hat{J}(\ell).$$

Thus, if $b > cK$, then all solutions to (20) decay to zero. We claim that if $z(x,0) = v(x,0) > 0$, then $z(x,t) > v(x,t)$ for all positive t. (We note that if $z(x_0,0) = v(x_0,0) = 0$ for some value of x_0, then both z_t and v_t will be positive due to the positive convolution term, so that both $z(x_0,t)$ and $v(x_0,t)$ will be positive for any positive t. Thus, we assume that the initial data are strictly positive.) If we can prove that $z > v$, then, since z decays to zero, so does $v(x,t)$ and thus so do all solutions to (19). Since $f(x) < -b$ for all x, it is clear that at $t = 0$, $v_t(x,0) < z_t(x,0)$ so that up to some time τ, $v(x,t) < z(x,t)$. Suppose at $t = \tau$ there is an x_0 with $v(x_0,\tau) = z(x_0,\tau)$. At that point of intersection, we must have $z_t(x_0,\tau) < v_t(x_0,\tau)$. But, since $z(x,\tau) \geq v(x,\tau)$ for all x,

$$\int_{\mathbb{R}} J(x-y)z(y,\tau)\ dy \geq \int_{\mathbb{R}} J(x-y)v(y,\tau)\ dy$$

and $-bz(x_0,\tau) > f(x_0)v(x_0,\tau)$, so from the evolution equations, $z_t(x_0,\tau) > v_t(x_0,\tau)$, a contradiction. Recalling that $b = \delta - cK$, we see that a sufficient condition for stability is that $-\delta + 2cK < 0$.

As we noted at the end of the existence proof, the quantity $-\delta + 2cK$ measures the competition between the attraction to the two different stable states (odd/even cycles of the stimulus) and the coupling which attempts to make the network uniform. We can use this result to motivate a more general result that is much more akin to the simulations in section 2. The parameter δ is related to the attractivity of the uncoupled states. Suppose that instead of the scalar function H we return to the general uncoupled periodically driven system:

$$\frac{du}{dt} = F(u,t),$$

where F is a general vector function which is T-periodic in its second argument. Suppose that $u_0(t)$ is a stable $2T$-periodic function representing a 1:2 locked solution. Since it is stable, all the Floquet exponents have negative real parts. Let $-\delta$ denote the real part of the exponent closest to zero real part. Then, we conjecture that there are regions locked to the even and odd cycles which persist as long as $\delta > cK$, where c is the coupling strength and K is a coupling function dependent value.

3.5. Traveling waves. In the previous sections, we proved the existence and linear stability of stationary solutions with discontinuities, as long as the coupling between cells is sufficiently weak. The experiments and our model show movement of the lines which indicates that the coupling strength must be fairly large. We can view the theory laid out in the last two subsections as being the mechanism for setting up the domains and assuring that they are stable. In this section we explore what happens in the simple model when the coupling increases.

Once again, reconsider (10), which we repeat here:

$$u_t(x,t) = H(u(x,t) + c\int_{\mathbb{R}} J(x-y)D(u(y,t) - u(x,t))dy.$$

We will relax our assumption that $J(x)$ is symmetric. We first prove the following proposition.

Proposition 1. *Suppose that* $H(\bar{u}) = 0$, $D(0) = 0$, $D'(0) > 0$, $J(x) \geq 0$, $c > 0$, *and* $\int_{\mathbb{R}} J(y)\, dy = 1$. *Then* $u(x,t) = \bar{u}$ *is a linearly stable solution to* (10).

Proof. Clearly, $\bar{u}$ is a solution to this equation. Linearizing about $\bar{u}$, we see that the linearized equation satisfies

$$v_t = -\delta v - cD'(0) + cD'(0)\int_{\mathbb{R}} J(x-y)v(y,t)\, dy.$$

Here $-\delta = H'(\bar{u})$. Solutions to this equation have the form

$$v(x,t) = e^{\lambda t}e^{ikx}.$$

The eigenvalue λ satisfies

$$\lambda = -\delta + cD'(0)[\hat{J}(k) - 1],$$

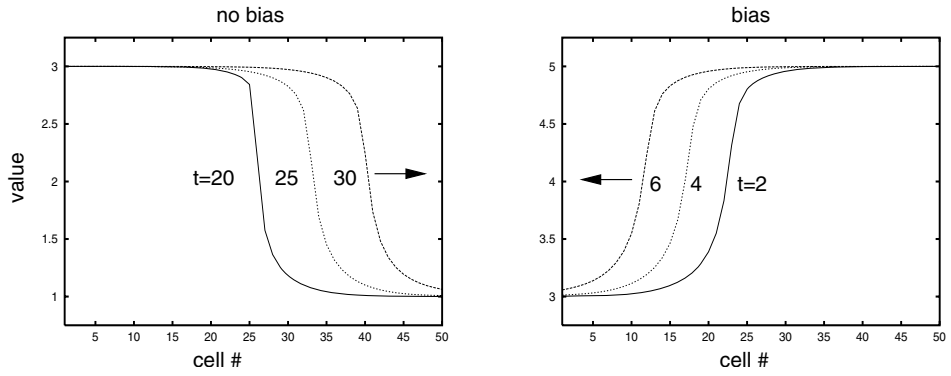

Figure 9. *Traveling wave simulation for* (10) *with* $H(u) = \sin \pi u$, $D(u) = \sin \pi u/2 + 0.25(1 - \cos \pi u/2)$, *and* $J(x) = \exp(-|x + p|)$ *on a grid of* $N = 50$ *cells. Coupling strength* $c = 6$. *Left:* $p = 0$, *no bias, shows the profiles in which the state* 3 *(equivalent to* -1 *on the periodic domain* $[0, 4)$*) takes over. Right: bias* $p = 0.25$ *leads to a wave traveling in the opposite direction.*

where $\hat{J}(k)$ is the Fourier transform of $J(x)$. Since $J(x) \geq 0$, $\Re\hat{J}(k) \leq \hat{J}(0) = 1$, so that

$$\Re\lambda < 0$$

for all k as long as $cD'(0) > 0$ and $\delta > 0$. Hence the constant state is stable.

Our assumptions on H presume that there are two stable constant solutions; thus, we expect that if the coupling is sufficiently strong, there will be a wave front switching from one state to the other. Indeed, if $D(u) = u$ was linear, then the existence, uniqueness, and stability of wave fronts would follow from a theorem of Chen [5]. Figure 9 shows an example simulation in which the -1 state takes over the $+1$ state when the coupling is large enough. This movement is due to a mechanism akin to that seen in Figure 5 for the nonbiased case. The interaction $J(x)$ is symmetric, but the function $D(u)$ is not a purely odd function. We can reverse the tendency for the $+1$ state to take over by allowing for asymmetric coupling. The right-hand side of Figure 9 shows a wave in which -1 takes over by making the coupling stronger from the right.

To gain some insight into the transition from stationary states to traveling waves, we use AUTO to explore the existence and stability of the stationary state as a function of the coupling strength. We consider $N = 20$ cells with nearest neighbor coupling:

$$u_j' = H(u) + c[(1 + s)D(u_{j-1} - u_j) + (1 - s)D(u_{j+1} - u_j)], \quad j = 1, \ldots, 20. \tag{21}$$

We set $u_0 = u_1$ and $u_{21} = u_{20}$ as the boundary conditions and choose functions $H(u) = \sin \pi u - 0.1 \cos \pi u$ and $D(u) = \sin \pi u/2 + 0.25(1 - \cos \pi u/2)$. We have added the cosine terms to make sure that the results do not depend on the oddness of the functions H, D. The parameter c is the overall coupling strength, and s is the measure of asymmetry. We choose $s = 0.1$ so that the left cell has a greater effect than the right cell. When $c = 0$, there are 2^N stable fixed points corresponding to each cell taking a value of either of the two stable roots to $H(u) = 0$ on the interval $[0, 4)$. (Since the cosine term for H is small, these roots are close to 1 and $3 = -1$.) Figure 10A shows the how the steady states evolve for

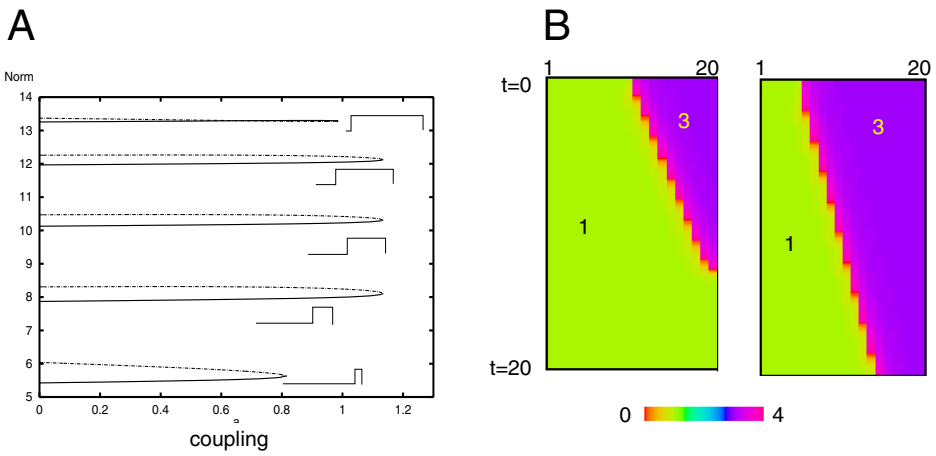

Figure 10. (A) *Bifurcation diagram for* (21) *for five different equilibrium states as the coupling, c, increases. Equilibria when* $c = 0$ *are shown to the right corresponding to cells in the* "1" *or* "3" *states.* (B) *Evolution of traveling waves for coupling larger than the critical value. Time increases downward, and cell index is horizontal. Coupling is stronger from the left so that the left state takes over the right. Left figure is for* $c = 1.3$ *such that the initial state has half the cells in the* "1" *state and the other half in the* "3" *state. Right panel is the same, but only the first five cells are in the* "1" *state.*

five different configurations. In each of the cases the first m cells are in the state near 1, and the remaining are in the state near 3. In all cases, as the coupling increases there is little quantitative change in the equilibria, but at a critical value of the coupling, the fixed point is lost at a saddle-node. If the distribution of cells is very unbalanced (say, only one cell in state 1 and the rest in state 3), then the amount of coupling required to destroy the steady state is small compared to the more balanced case. An analogue of this is seen in Figure 8C,D, where the thin region between two similar domains is quickly absorbed. Figure 10B shows the evolution of the stationary state when the coupling is larger than the saddle-node value. The left figure shows that in the balanced case, as expected from the coupling bias, the "1" state takes over the "3" state. Even when there is a 3:1 advantage of "3" state, the bias is able to overcome this, and a traveling wave results. When only the leftmost cell is in the "1" state and the other cells are in the "3" state, then the wave travels to the left—the bias is unable to overcome the huge unbalance.

4. Discussion. We have derived a simple model for complex visual effects due to the direct stimulation of the eyeball. The model is based on the simple idea that if there is phase-locking between a stimulus which fires twice for every response of the cell, then there is a natural bistability in the medium: firing on the odd or even cycles of the stimuli. We have suggested that visual stimuli are able to push the phase-locked retinal cells into different basins of attraction and that the boundaries between the bistable domains account for the thin line illusions. This notion allows us to make several predictions. First, the thickness of the boundaries should be independent of any stimulus properties—the "boundary layer" is, rather, a function of the intrinsic coupling between retinal cells involved in the illusion. Stronger coupling should lead to thicker boundaries. Second, more complex patterns should be easy to create. For example, a visual stimulus consisting of an expanding annulus should

result in a series of concentric circular patterns which will gradually disperse. Third, the illusion should disappear instantly when the electrical stimulus is cut off, since the cells will no longer fire and there will thus be no phase boundary. We have not completely explored how differently shaped electrical stimuli will affect the patterns. However, one important prediction that we can make is that if the electrical stimulation is at a sufficiently low frequency, there will be no illusion, since the retinal cells will be able to fire in a 1:1 manner and so no phase-boundaries can develop. This would allow us to distinguish our model from the model of Willis, which we discuss briefly below.

In addition to a biologically "realistic" model, we abstracted the mechanism to a scalar bistable medium with nonlocal but "weak" coupling. We proved a theorem about the existence and stability of patterned states, and then explored how asymmetric coupling which is sufficiently strong can lead to traveling waves that connect the stable states of the bistable medium, similar to those in [11].

There has been one other attempt to model these curious phosphenes [22]. The Willis model captured the idea of bistability but did not model the slow movement of the phosphenes over time. Willis' model is based on a piecewise linear firing rate model, which proposes that the interactions between two classes of cells (receptors and horizontal cells) switch sign (excitation becomes inhibition and vice versa) during the two phases of electrical excitation. Unless the nonlinearities of the Willis model are exactly balanced, one of the two states should have a larger basin of attraction than the other. Thus, with any coupling at all, in the Willis model, we would expect the phosphenes to have a strong tendency to move in a preferred direction. This is not reported in the experiments. Our model is considerably simpler and makes fewer assumptions about the cells and their connectivity. The two models could be experimentally distinguished by recording from ganglion or horizonal cells during the phosphenes. While this is unlikely, given that the subjects are humans, our model is more compatible with both the physiological data in salamanders and the psychophysical data in humans [7]. Furthermore, the Willis model would predict that the phosphenes persist at lower frequencies, say, 50 Hz, since the bistability is based on a different mechanism from ours. This is easy to test in humans.

While the illusions we have modeled are unusual and a consequence of unnatural stimuli, such experiments can often be used to shed light on basic biological structure and function. For example, by probing the retina with periodic stimuli, we can determine the frequency response of the neurons. The width of the phosphenes tells us something about the degree of intrinsic connectivity between retinal cells. Finally, there is a good deal of recent interest in direct stimulation of the nervous system as a means of providing visual prosthesis [14]. Thus, models such as the present one can provide a simple framework for exploring how direct electrical stimuli are visually interpreted.

REFERENCES

[1] D. Attwell, *Interaction of low frequency electric fields with the nervous system: The retina as a model system*, Radiat. Prot. Dosimetry, 106 (2003), pp. 341–348.

[2] P. Bates and A. Chmaj, *An integrodifferential model for phase transitions: Stationary solutions in higher space dimensions*, J. Statist. Phys., 95 (1999), pp. 1119–1139.

[3] G. S. Brindley, *The site of electrical excitation of the human eye*, J. Physiol., 127 (1955), pp. 189–200.
[4] R. H. S. Carpenter, *Contour-like phosphenes from electrical stimulation of the human eye: Some new observations*, J. Physiol., 229 (1973), pp. 767–785.
[5] X. Chen, *Existence, uniqueness, and asymptotic stability of traveling waves in nonlocal evolution equations*, Adv. Differential Equations, 2 (1997), pp. 125–160.
[6] J. Claussen, *Visual sensations (phosphenes) produced by AC sine wave stimulation*, Acta. Psychiatr. Neurol. Scand. Suppl., 94, pp. 1–10.
[7] D. Crevier and M. Meister, *Synchronous period-doubling in flicker vision of salamander and man*, J. Neurophysiol., 79 (1998), pp. 1869–1878.
[8] P. Dayan and L. Abbott, *Theoretical Neuroscience*, MIT Press, Cambridge, MA, 2001.
[9] J. Drover, *The Interplay of Intrinsic Dynamics and Coupling in Spatially Distributed Neuronal Networks*, Ph.D. thesis, Mathematics Department, University of Pittsburgh, Pittsburgh, PA, 2005; available online at http://etd.library.pitt.edu/ETD/available/etd-08162005-135431.
[10] G. B. Ermentrout, *n:m phase-locking of weakly coupled oscillators*, J. Math. Biol., 12 (1981), pp. 327–342.
[11] B. Ermentrout, X. Chen, and Z. Chen, *Transition fronts and localized structures in bistable reaction-diffusion equations*, Phys. D, 108 (1997), pp. 147–167.
[12] S. I. Firth, C.-T. Wang, and M. B. Feller, *Retinal waves: Mechanisms and function in visual system development*, Cell Calcium, 37 (2005), pp. 425–432.
[13] J. R. Gibson, M. Beierlein, and B. W. Connors, *Functional properties of electrical synapses between inhibitory interneurons of neocortical layer* 4, J. Neurophysiol., 93 (2005), pp. 467–480.
[14] L. E. Hallum, G. J. Suaning, and N. H. Lovell, *Contribution to the theory of prosthetic vision*, ASAIO J., 50 (2004), pp. 392–396.
[15] S. Hidaka, T. Kato, and Y. Hashimoto, *Structural and functional properties of homologous electrical synapses between retinal amacrine cells*, J. Integr. Neurosci., 4 (2005), pp. 313–340.
[16] E. H. Hu and S. A. Bloomfield, *Gap junctional coupling underlies the short-latency spike synchrony of retinal alpha ganglion cells*, J. Neurosci., 23 (2003), pp. 6768–6777.
[17] G. T. Kenyon and D. W. Marshak, *Gap junctions with amacrine cells provide a feedback pathway for ganglion cells within the retina*, Proc. Biol. Sci., 265 (1998), pp. 919–925.
[18] N. Kopell and G. B. Ermentrout, *Symmetry and phaselocking in chains of weakly coupled oscillators*, Comm. Pure Appl. Math., 39 (1986), pp. 623–660.
[19] T. J. Lewis and J. Rinzel, *Self-organized synchronous oscillations in a network of excitable cells coupled by gap junctions*, Network, 11 (2000), pp. 299–320.
[20] F. Ratliff, *Mach Bands: Quantitative Studies on Neural Networks of the Retina*, Holden-Day, San Francisco, 1965.
[21] C. W. Tyler, *Some new entoptic phenomena*, Vision Res., 18 (1978), pp. 1633–1639.
[22] J. B. Willis, *The modeling of neural circuitry*, Progr. Neurobiol., 26 (1986), pp. 93–118.
[23] M. Wilms, M. Eger, T. Schanze, and R. Eckhorn, *Visual resolution with epi-retinal electrical stimulation estimated from activation profiles in cat visual cortex*, Vis. Neurosci., 20 (2003), pp. 543–555.
[24] H. R. Wilson, *Computational evidence for a rivalry hierarchy in vision*, Proc. Natl. Acad. Sci. USA, 100 (2003), pp. 14499–14503.